Vertical angular momentum constraint on lunar formation and orbital history

ZhenLiang Tian[a,b,1,2] and Jack Wisdom[c,1,2]

[a]Department of Earth and Planetary Sciences, University of California, Santa Cruz, CA 95064; [b]Department of Earth and Space Sciences, Southern University of Science and Technology, Shenzhen 518055, China; and [c]Department of Earth, Atmospheric, and Planetary Sciences, Massachusetts Institute of Technology, Cambridge, MA 02139

Contributed by Jack Wisdom, May 4, 2020 (sent for review February 25, 2020; reviewed by Robin M. Canup and Scott Tremaine)

The Moon likely formed in a giant impact that left behind a fast-rotating Earth, but the details are still uncertain. Here, we examine the implications of a constraint that has not been fully exploited: The component of the Earth–Moon system's angular momentum that is perpendicular to the Earth's orbital plane is nearly conserved in Earth–Moon history, except for possible intervals when the lunar orbit is in resonance with the Earth's motion about the Sun. This condition sharply constrains the postimpact Earth orientation and the subsequent lunar orbital history. In particular, the scenario involving an initial high-obliquity Earth cannot produce the present Earth–Moon system. A low-obliquity postimpact Earth followed by the evection limit cycle in orbital evolution remains a possible pathway for producing the present angular momentum and observed lunar composition.

moon formation | orbital evolution | angular momentum

Recent giant-impact simulations (1–3) aimed at producing a Moon with an Earth-like isotopic composition (4–8) would leave the postimpact Earth rotating too fast. Some subsequent process must be responsible for draining the excess angular momentum (AM).

Ćuk and Stewart (1) proposed that the excess AM could be drained by the lunar orbit's temporary capture into the evection resonance (9). Wisdom and Tian (10) found that the evection limit cycle can also do the job. While ref. 10 used the Darwin–Kaula constant Q tidal model (*SI Appendix*, *Model Comparison*), Rufu and Canup (11) found similar phenomena using the constant Δt tidal model. Tian et al. (12) studied the consequences of tidal heating in these resonance and near-resonance mechanisms and found that the evection resonance is unstable and therefore unable to drain enough AM, whereas the evection limit cycle is stable and continues to drain AM.

Instead of starting the postimpact fast-spinning Earth with a small obliquity (I_e), Ćuk et al. (13) proposed that the giant impact left the Earth in a high-obliquity (I_e = 65 to 80°), fast-spinning state. They suggested that the subsequent evolution could not only drain the excess AM through an instability associated with the Laplace plane transition (LPT), but also solve the long-standing puzzle of the present-day lunar inclination ($i^p = 5^\circ$, where i is the lunar inclination, and the p superscript denotes the present-day value) (9, 14, 15). When the Moon is close to the Earth, the lunar precessional motion is strongly affected by the oblateness of the Earth, but when the Moon is far from the Earth, the precessional motion is more strongly affected by solar perturbations. The LPT occurs when these two effects are comparable. The LPT instability occurs only when I_e reaches large values during the LPT (16, 17). The high I_e leads to nonzero orbital eccentricities via Lidov–Kozai-like oscillations and temporary contraction of the lunar orbit, during which substantial AM is removed from the Earth–Moon.

However, there exists a nearly conserved quantity, which has so far not been taken into account, that significantly constrains the possible evolutionary histories of the Earth–Moon system.

A New Constraint: Vertical AM

For a test particle around a central mass with large eccentricity (e) and inclination (i), nonresonant perturbation from a massive exterior body moving in a circular orbit induces oscillations in e and i, the Lidov–Kozai oscillations (18, 19). In the nontidal Lidov–Kozai problem, the Hamiltonian governing the system evolution is averaged over the orbital periods of both the test particle and the perturber. This leads to a conservation of the semimajor axis (a) of the test particle, and the component of the orbital AM of the test particle that is perpendicular to the orbital plane of the massive perturber, which we refer to as L_z^{orb}. Taking the orbital plane of the massive perturber as the reference plane for inclination, then $L_z^{orb} \propto \sqrt{a(1-e^2)}\cos i$. The conservation of a and L_z^{orb} implies that as e and i oscillate, the quantity $\sqrt{1-e^2}\cos i$ is conserved (the Lidov–Kozai constant).

The motion of the Earth–Moon system has much richer dynamics than the three-body problem. Perturbations to the system come from not only the Moon–Sun interaction, but also the Earth's oblateness, which leads to precession of the Earth's spin axis and contributes to lunar-orbit precession; the Moon's permanent triaxial figure, which allows the Moon to maintain synchronous rotation; and the Moon's oblateness and triaxiality, which dictates the equilibrium obliquity of the Moon (the Cassini states)—not to mention the tides on the Earth and Moon. These processes modify the orbital AM of the Moon and the rotational AM of the Earth. Nevertheless, there is a quantity analogous to the Lidov–Kozai constant, the vertical component of the AM of the Earth–Moon system (L_z), that is conserved if resonances between the Sun and the Earth or Moon are not encountered. For instance, the evection resonance and the evection limit cycle

Significance

There are various scenarios for the formation of the Moon and subsequent dynamical evolution of the Earth–Moon system, all of which are subject to a constraint that has not previously been fully exploited. Using this constraint, we demonstrate that the recently proposed high-obliquity scenario is not consistent with the present Earth–Moon system. This constraint will have to be taken into account in all future investigations of the formation and evolution of the Moon.

Author contributions: Z.T. and J.W. designed research, performed research, analyzed data, and wrote the paper.

Reviewers: R.M.C., Southwest Research Institute; and S.T., Institute for Advanced Study.

The authors declare no competing interest.

Data deposition: The computer codes we used for the simulations in this paper are available at GitHub, https://github.com/zhenliangtian/em3d.

[1]Z.T. and J.W. contributed equally to this work.

[2]To whom correspondence may be addressed. Email: wisdom@mit.edu or zlt@ucsc.edu.

This article contains supporting information online at https://www.pnas.org/lookup/suppl/doi:10.1073/pnas.2003496117/-/DCSupplemental.

(1, 10–12) can modify L_z. Such resonances or near-resonances are absent in scenarios like the LPT instability, which we term as nonresonant scenarios. The demonstration of the conservation of L_z for nonresonant scenarios exactly follows the derivation for the Lidov–Kozai problem (*SI Appendix, SI Text*). The Hamiltonian is averaged over the orbital period of the Moon and the orbital period of the motion of the Earth about the Sun. The average over the lunar period leads to the conservation of the semimajor axis of the Moon. The average over the motion of the Earth about the Sun leads to the conservation of L_z. Tides between the Earth and Moon conserve L_z, but induce long-term changes in a and the other system parameters.

The AM of the Earth–Moon system $\vec{L}$ is approximately $\vec{L}^{\oplus} + \vec{L}^{\leftmoon}$, where $\vec{L}^{\oplus}$ is the rotational AM of the Earth and $\vec{L}^{\leftmoon}$ is the orbital AM of the Moon. Here, we are neglecting the small rotational AM of the Moon. Taking the ecliptic as the reference plane, the component of AM perpendicular to this plane is

$$L_z = L^{\oplus} \cos I_e + L^{\leftmoon} \cos i, \qquad [1]$$

where $L^{\oplus}$ is the magnitude of $\vec{L}^{\oplus}$, and $L^{\leftmoon}$ is the magnitude of $\vec{L}^{\leftmoon}$. We denote the scalar sum $L^{\oplus} + L^{\leftmoon}$ by L_s.

In our model, which includes the full rotational and orbital dynamics of the Moon, interacting with an oblate, precessing Earth on a near circular orbit about the Sun, with tidal interactions between the Moon and Earth, we find that L_z is conserved to a part in a thousand, as the Moon evolves from $5R_e$ to $50R_e$ (where we terminate the integrations; R_e = 6,371 km). This is the case, even though the system passes through the instability associated with the LPT and the Cassini state (lunar spin) transitions. Touma and Wisdom (20) investigated the evolution in a model that was, in a number of ways, more complete than that used here. That model included a fully evolving eccentric and inclined Earth orbit, perturbed by all of the chaotically evolving planets, with not only tidal interactions between the Earth and Moon, but also direct tides from the Sun on the Earth, and cross-tidal interactions from tides raised on the Earth by the Sun that affect the Moon. (But it did not include tides raised on the Moon and the rotational dynamics of the Moon, which are included here.) A reexamination of those results shows that, even with all these additional effects, L_z was still conserved to about 3.5% (Fig. 1). (Note that refs. 16, 20, and 21 already recognized that L_z is conserved in the averaged $e = 0$ nontidal case, and refs. 16 and 20, in addition, stated that L_z is conserved if only tides between the Earth and Moon are considered. Our derivation is more general.) We show in *SI Appendix, SI Text* that even without averaging, when solar tides are ignored, the amplitude of oscillation of L_z is at most of order $10^{-3}L_r$ in Earth–Moon history (*SI Appendix*, Eq. **S11** and Fig. S2) ($L_r = C_e^p \sqrt{GM_e R_e^{-3}}$ is the reference AM, where C_e is Earth's largest principal moment, $C_e^p = 0.3308 M_e R_e^2$ is the present-day value, M_e is Earth's mass; $L_s^p = 0.345 L_r$ and $L_z^p = 0.339 L_r$).

Apart from the dynamical evolution, L_z is also susceptible to small changes due to collisional processes after the Moon-forming giant impact, e.g., the stochastic late-accretional impacts on Earth that are proposed to explain the presence of highly siderophile elements in the terrestrial mantle (22–26). These impacts can change the Earth's rotational AM by up to 4%, with the Earth rotating with a period between 6 and 8 h (22). Taking $C_e \approx C_e^p$, the change in $L^{\oplus}$ is $\Delta L^{\oplus} \approx C_e^p \cdot 2\pi/(7\text{hr}) \cdot 4\% = 8 \times 10^{-3} L_r$, i.e., 2.3% of L_s^p. The late impacts on the Moon are much smaller in volume, and their effects on the system AM can be ignored. Even if the change in $\vec{L}^{\oplus}$ is perfectly aligned to the vertical direction, this will only cause changes to L_z by up to $2.4\% \cdot L_z^p$ (either increase or decrease). So we ignore these possible late stochastic variations in L_z.

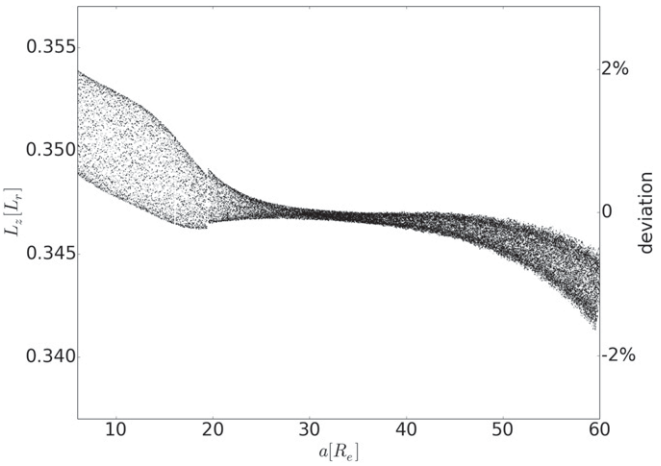

Fig. 1. L_z versus a for a simulation in ref. 20, which evolves the Earth–Moon system with solar tides, Earth–Moon mutual tides, and Sun–Earth–Moon cross tides, in the full chaotically evolving planetary system, using the constant Δt tidal model. The system begins with a conventional initial state, instead of a high-AM state. L_z declines by only 3.5% throughout the evolution.

Therefore, we can take L_z conservation as a strong constraint on the evolution of the Earth–Moon system. For nonresonant scenarios of Earth–Moon formation and evolution (e.g., ref. 13), the postimpact L_z value should be near L_z^p (at most a few percent different). For models of Earth–Moon history that involve resonances related to Earth's motion about the Sun (e.g., refs. 1 and 10–12), the postresonance L_z should be near L_z^p in the same way.

L_z Constraint on the High-Obliquity Scenario

Čuk et al. (13) argued that following a high-AM, high-obliquity postimpact Earth, the present-day AM, I_e and i can be produced through nonresonant orbital evolution. However, the values of L_z for their initial conditions were much lower than L_z^p (*SI Appendix*, Table S1 and Figs. S1 and S4) and therefore inconsistent with the present Earth–Moon system.* We investigate the high-obliquity Moon-forming scenario with the L_z constraint taken into account. Our numerical model is exactly the same as used in ref. 10. It is based on the N-body symplectic mapping algorithm (27) and the conventional Darwin–Kaula constant Q model (28). We provide a detailed comparison of our algorithm to that of ref. 13 in the *SI Appendix, Model Comparison*. As a check, we did calculations with the same initial conditions as used in ref. 13. The main features of ref. 13 are reproduced, but some differences are found. We find smaller final L_s, with larger final I_e and i (*SI Appendix*, Figs. S1, S3, and S4).

We sample the L_z-consistent (i.e., $L_z = L_z^p$) initial conditions (postimpact states) in the whole range of successful high-AM giant impact simulations; I_e, i, and L_s are of key interest. We assume that the Moon accreted on the Earth's equatorial plane, i.e., initially $i = I_e$. We take the initial $a = 3.5R_e$, just outside the Earth's Roche limit. So (I_e, L_s) adequately represents an initial state. In ref. 1, for successful impacts, L_s ranges in 1.94 to $2.84 L_s^p$ or 0.67 to $0.98 L_r$. Candidate impacts in ref. 2 produce L_s from 1.77 to $2.71 L_s^p$ or 0.61 to $0.94 L_r$. With the constraint of $L_z = L_z^p$,

*Even though Ćuk et al. (13) tried to match the present-day AM, I_e, and i, the L_z values were not L_z^p. They simulated the Earth–Moon history in two steps, first for $a \le 25R_e$ and then for $25R_e < a \le 60R_e$. After the first step, AM and I_e get close to the present values, but i is still much larger than $i^p = 5^\circ$. Then, in the second step, they concentrated on reducing i to i^p, but did not track I_e. Actually, I_e will increase in the second step, so the final state will not match the present values of AM, I_e, and i.

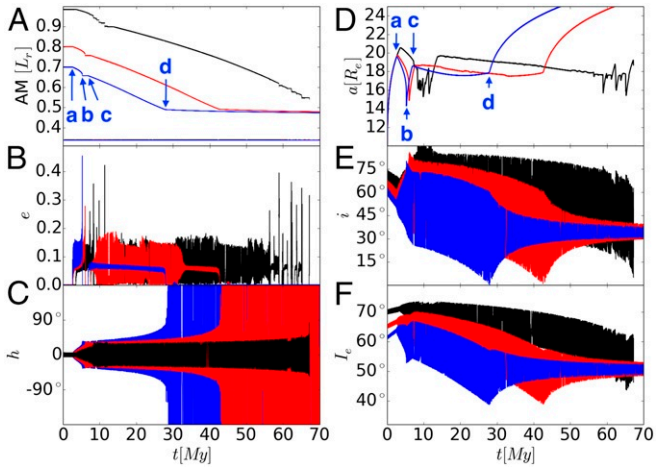

Fig. 2. Details of LPT [(*A*) angular momentum, (*B*) lunar eccentricity, (*C*) the angle between the ascending node of the lunar orbit and the ascending node of the Earth's equator, (*D*) lunar semimajor axis, (*E*) lunar inclination, and (*F*) Earth's obliquity], with L_z-consistent initial conditions (in [I_e, L_s]): (61°, 0.7L_r [blue]), (65°, 0.8L_r [red]), (70°, 0.98L_r [black]). Parameters are as follows: $Q_e/k_{2e} = 100$, $Q_m/k_{2m} = 100$. In *A*, the top lines are L_s ($=L^{\oplus} + L^{☾}$), and the horizontal line is L_z ($=L_z^{\oplus} + L_z^{☾}$). The fact that the L_z line is horizontal indicates that it is conserved by the evolution. Most of the decline in L_s occurs when both *e* is nonzero and *h* oscillates. For the blue curves, a and d mark the beginning and end of the LPT.

we take four sampling points: $(57.6°, 0.63L_r)$, $(61°, 0.7L_r)$, $(65°, 0.8L_r)$, and $(70°, 0.98L_r)$. A larger initial I_e corresponds to a larger initial L_s. We take $Q_e/k_{2e} = 100$ and $Q_m/k_{2m} = 100$, the values used in ref. 13, where k_2 is the potential Love number, and Q is the tidal quality factor.

In the case $(57.6°, 0.63L_r)$, I_e does not get large enough for the instability during the LPT (17), so the AM is not decreased.

Results for the $(61°, 0.7L_r)$, $(65°, 0.8L_r)$, and $(70°, 0.98L_r)$ cases are shown in Fig. 2. In the $(70°, 0.98L_r)$ case, there are a lot of sudden, large excursions in eccentricity, and it ends with an unbound orbit. All of the cases end with a high $L_s \sim 0.5L_r$, 45% larger than the present value of $0.345L_r$. The Earth's obliquity after the LPT, around 50°, is too large to produce the present I_e of 23.4° in the later evolution (*SI Appendix, Low-e Phases of Evolution*). The post-LPT inclination being high ($\sim 34°$) may not be a problem, since it can be damped during the subsequent Cassini-state transition, provided that the lunar magma ocean has not solidified by that point (29). However, conservation of L_z implies that if the inclination is damped, then the obliquity must increase, making it even more difficult to produce the present I_e.

Since these initial conditions are representative of all possible combinations of post-giant-impact I_e and L_s, these results show that, with $L_z = L_z^p$, the high-obliquity scenario does not work to produce the present-day AM and Earth's obliquity, at least for the tidal parameters used ($Q_e/k_{2e} = 100$ and $Q_m/k_{2m} = 100$). Next, we show that this is the case regardless of the tidal model and tidal parameters.

Characteristics of the High-I_e Scenario

The decrease in L_s (AM scalar sum) occurs predominantly during the LPT instability, during which the lunar eccentricity is nonzero and the semimajor axis, a, stalls. The rate of change of a (da/dt) is a competition between tides on Earth (which tend to increase a) and tides on the Moon (which tend to decrease a). At zero e, da/dt is positive. But da/dt decreases as e is increased (e.g., ref. 10). There is an e at which da/dt is zero. The value of e at this point depends on a ratio of the tidal parameters of the Earth and Moon and the tidal model. Though the expressions in ref. 10 need to be generalized, they give a rough estimate of the value of e for $da/dt = 0$ that is consistent with our simulations and tidal parameters.

During the phase in which $da/dt \approx 0$, L_s declines. We can calculate the rate of decline if we assume $da/dt = 0$. In this case, the changing part of L_s is predominantly the rotational AM of the Earth. The rate of change of AM is the component of the tidal torque on the spin axis of the Earth. Though the tidal torque depends on many factors, the leading term, T_0, sets the timescale and depends only on parameters and the semimajor axis. This term is the same for the constant Q tidal model and the constant Δt tidal model (20):

$$T_0 = -\frac{3}{2}\frac{k_{2e}}{Q_e}\frac{GM_m^2R_e^5}{a^6}, \qquad [2]$$

where M_m is the mass of the Moon. Using the expression for the reference AM L_r, we find

$$\frac{d}{dt}\frac{L_s}{L_r} = -\frac{3}{2}\frac{1}{\lambda}\frac{k_{2e}}{Q_e}\left(\frac{M_m}{M_e}\right)^2\left(\frac{R_e}{a}\right)^{9/2} n, \qquad [3]$$

where $\lambda = 0.3308$ is the present moment of inertia of the Earth divided by $M_eR_e^2$, and n is the mean motion of the lunar orbit. Evaluating this expression for $a = 18R_e$, we find, independent of tidal models, a decline of about 7.9×10^{-3} per million years (My). The decline found in the simulations is comparable to this, about 7.8×10^{-3} per My. The agreement is excellent. This success allows us to generalize our simulation results to other tidal parameters. The rate of decline of L_s/L_r is simply proportional to k_{2e}/Q_e. With a larger Q_e, we can expect that it would take longer to leave the LPT, but that the ending value of L_s/L_r would be roughly the same (see below).

Termination of the LPT is marked by a change in the behavior of the angle between the ascending node of the lunar orbit on the ecliptic (Ω) and the ascending node of the Earth's equator on the ecliptic (h_0); we denote this angle by h ($=\Omega - h_0$). During the LPT, h oscillates about 0; after exit from the LPT, h circulates through all angles (Fig. 2). The point of transition from oscillation to circulation of h is well defined. At this point,

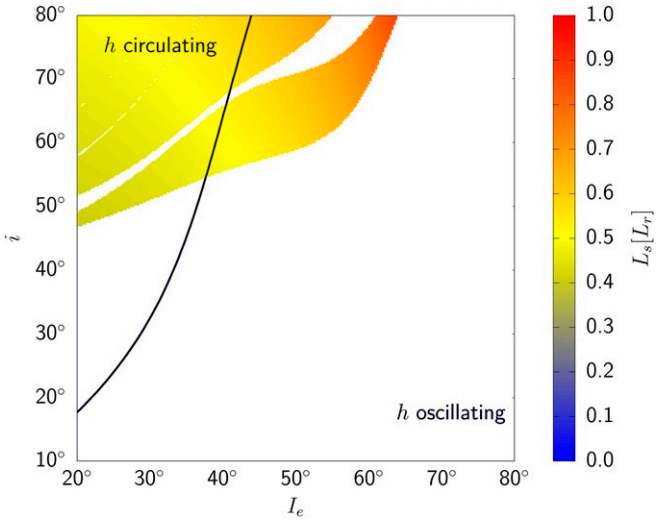

Fig. 3. The stability diagram for $a = 18R_e$ plots the color corresponding to the value of L_s/L_r if the circular orbit is linearly unstable. The black line marks the boundary between oscillating *h* and circulating *h*. L_s/L_r can only decrease if the system is in the unstable region with *h* oscillating. There is a small "disconnected" arc-like unstable region with smaller I_e and *i* that is not shown, because it cannot be reached by tidal evolution.

Table 1. Minimum L_s/L_r obtained while the system is undergoing the LPT instability, at different semimajor axis values

a [R_e]	L_s^{min} [L_r]	I_e^{min}
16	0.437	29°
17	0.452	33°
18	0.472	38°
19	0.498	43°
20	0.496	47°

the semimajor axis resumes its outward evolution. Though there is a brief interval in which e is still nonzero after this point, the decline of L_s is small. Once e decays to zero, L_s changes very little.

We can determine the lowest value of L_s that can be obtained during the LPT instability by systematically exploring the behavior of the averaged, nontidal Earth–Moon system. For e to be nonzero, the circular orbit must be unstable; otherwise, the orbit will stay circular ($e=0$) and not get elliptical ($0<e<1$). To be in the LPT instability, h must oscillate. So we can determine the minimum L_s that can be obtained by systematically finding all L_z-consistent states that satisfy two conditions: 1) $e=0$ is unstable, and 2) h oscillates. If the minimum L_s determined in this way is much larger than L_s^p, then the high-I_e scenario is not consistent with the present Earth–Moon system. The conclusion is independent of tidal models and tidal parameters.

The Hamiltonian describing the evolution of the nontidal Earth–Moon system, averaged over the orbital timescales of the Earth and Moon, denoted as $\mathscr{H}_{EM}$, is shown in *SI Appendix, SI Text*. $\mathscr{H}_{EM}$ is very similar to the Hamiltonian derived in Touma and Wisdom (20), but is generalized to arbitrary nonzero eccentricity. For the averaged system, three quantities are conserved: L_z, a, and Earth's rotation rate. Then, $\mathscr{H}_{EM}$ has two degrees of freedom (or a four-dimensional phase space).

Since the Hamiltonian has two degrees of freedom, it is natural to study the evolution with surfaces of section, which reveal the phase-space structure and determine the stability of fixed points (30). The values of the three conserved quantities must be specified for each section. We set $L_z=L_z^p$ for all sections. We make a stability diagram for each a. On this stability diagram, initial values of I_e and i are chosen, for $h=0$ and $e=0$. From these, we determine the Earth's rotation rate and the value of the Hamiltonian. Since $\mathscr{H}_{EM}$ has no time dependence, it is conserved. All points on a section share the same $\mathscr{H}_{EM}$ value.

We take the axes of the surface of section to be $x=e\cos\omega$ and $y=e\sin\omega$, where ω is the argument of pericenter of the lunar orbit. The section condition is $h=0$ (restricted to the $\dot{h}<0$ case). The value of the momentum conjugate to h is determined by requiring that $\mathscr{H}_{EM}$ has the chosen value. The return map is obtained by integrating the evolution until the section condition $h=0$ ($\dot{h}<0$) is again satisfied. The map from the pair (x,y) to the next (x,y) defines the return map P.

Linear stability analysis of the map P determines the stability of the fixed point $(0,0)$ (at $e=0$) (30). We make a stability diagram for a specified a (e.g., Fig. 3). For the initial values of I_e and i, if the fixed point $(0,0)$ is unstable, then a color corresponding to the value of L_s/L_r is plotted. A black line marks the boundary between h oscillating and h circulating. For L_s/L_r to decline substantially, $e=0$ must be unstable, and h must be oscillating.

The stability diagram for $a=18R_e$ is shown in Fig. 3. The minimum value of L_s/L_r satisfying both conditions is 0.47, which is significantly larger than the present value of 0.34. The minimum Earth obliquity reached is about 38°, much larger than the 20° post-LPT obliquity that is required for subsequent evolution to reach the present 23.4° (*SI Appendix*, , *Low-e Phases of Evolution*). The results for other values of a are shown in Table 1. L_s^{min} and I_e^{min} are the minimum L_s and obliquity in the unstable e, oscillating h regions, such as the colored region in Fig. 3. Notice that the predicted L_s^{min} agrees well with the minimum L_s obtained in our simulations (Fig. 2). We see that with L_z set at L_z^p, the high-I_e scenario is not able to produce the present Earth–Moon system, regardless of tidal parameters and tidal models. The present-day lunar inclination i^p remains a puzzle.

Even though the stability diagrams are for the nontidal averaged system, they suggest what the tidal evolution through the LPT instability would look like on the I_e–i plane. The system begins with large I_e and i. As it evolves into the region of the LPT instability, the system enters the colored tongues of instability and develops nonzero eccentricity. At this point, the system begins to undergo large variations in I_e and i, while maintaining roughly constant a (the system roughly stays on the stability diagram). These large oscillations in I_e and i are reminiscent of those found by Atobe and Ida (16) in the $e=0$ case. Tidal torques reduce L_s/L_r, and the system proceeds down the tongue of instability (diagonally toward the lower left). But once the boundary between h oscillation and circulation is reached, the system changes course and soon leaves the LPT instability. There is no further significant reduction in L_s/L_r.

Examination of the simulations confirms this picture (Fig. 4). Whenever $|h|<0.03$ radians, with $\dot{h}<0$, we plot a point on the $i-I_e$ plane. The semimajor axis is not constant in the simulations, so we indicate the value of a by a color. The evolution begins in the upper right. Once the system enters the LPT instability, the semimajor axis a is roughly constant. During this phase, the colors are orange to yellow. The system evolves down diagonally to the left until the boundary between h oscillation and circulation is reached. At this point, the trajectory on the plot changes direction. The semimajor axis then resumes its outward evolution, as indicated by the change of

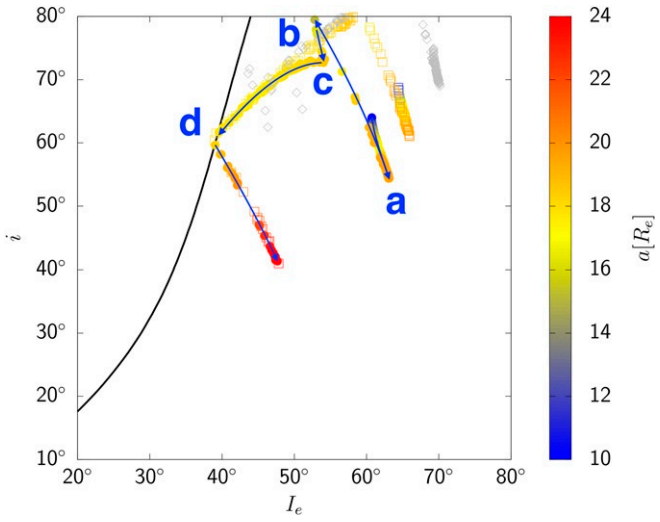

Fig. 4. i versus I_e whenever $|h|<0.03$ radians and $\dot{h}<0$ for the simulations shown in Fig. 2, with initial conditions (in [I_e, L_s]): (61°, 0.7L_r [circle]), (65°, 0.8L_r [square]), and (70°, 0.98L_r [diamond]). The color indicates the value of a. Note that the three simulations, though started with different initial conditions, merge onto a common track. The black line marks the boundary between h oscillating (to the right) and h circulating for $a=18R_e$. For the simulation with initial $I_e=61°$, the arrows show the direction of time evolution, and the marks a–d correspond to the points in Fig. 2 with the same labels.

color to red. In this final phase, the stability diagram at fixed a no longer applies. The eccentricity damps to zero, and L_s no longer declines substantially.

L_z Constraint on Resonant Scenarios

The evection resonance and the evection-limit cycle involve a resonance between the precession of the lunar pericenter and the motion of the Earth around the Sun. Substantial AM can be lost in the form of a decrease in L_z (1, 10–12). However, L_z is conserved in the postresonance evolution. The late-accretional impacts can only modify L_z by up to $8 \times 10^{-3} L_r$ (either increase or decrease). Even the presence of solar tides and planetary perturbations can only decrease L_z as much as $0.01 L_r$. Therefore, for a scenario of evection resonance or evection limit cycle to be a possible representation of the Earth–Moon history, the postresonance state should have its L_z close to L_z^p ($0.339 L_r$): $0.331 L_r < L_z < 0.357 L_r$.

The evection resonance (1) and the near-resonance described in ref. 11 both involve high lunar eccentricities (> 0.5). Such high eccentricities will lead to severe heating in the Moon and cause these mechanisms to quickly exit with little AM decreased (12). The evection limit cycle (near-resonance) described in refs. 10 and 12 leads to lower eccentricities and is thermally stable (12). However, the post-limit cycle minimum L_z is $0.393 L_r$ in ref. 10 and $0.404 L_z$ in ref. 12, both with $Q_e = 400$. It was then thought that the subsequent evolution would decrease L_z, but the L_z constraint rules out this possibility.

It was found in ref. 12 that a smaller L_z can be produced with a larger Q_e (0.436, 0.404, and 0.389 L_r for Q_e = 300, 400, and 500). With a large Q_e (10^3 to 10^4) in the early history of the Earth (31), the evection limit cycle remains a possible mechanism to drain the excess AM from a fast-spinning Earth.

Code Availability

The computer codes we used for the simulations in this paper are available at GitHub, https://github.com/zhenliangtian/em3d.

Conclusion

The L_z constraint places limits on the possible orbital histories of the Earth–Moon system and thus limits the details of the Moon-forming giant impact. For a high-AM impact (1–3), which is able to produce a Moon with an Earth-like composition, the impact geometry is constrained to cases where the postimpact Earth has a small to medium obliquity.

ACKNOWLEDGMENTS. This research was initiated in anticipation of the Moon Workshop, held October 14–16, 2019, at the American University of Beirut, Lebanon, organized by Jihad Touma. We thank Francis Nimmo for helpful discussions.

1. M. Ćuk, S. T. Stewart, Making the Moon from a fast-spinning Earth: A giant impact followed by resonant despinning. *Science* **338**, 1047–1052 (2012).
2. R. M. Canup, Forming a Moon with an Earth-like composition via a giant impact. *Science* **338**, 1052–1055 (2012).
3. S. J. Lock *et al.*, The origin of the Moon within a terrestrial synestia. *J. Geophys. Res. Planets* **123**, 910–951 (2018).
4. G. W. Lugmair, A. Shukolyukov, Early solar system timescales according to ^{53}Mn-^{53}Cr systematics. *Geochim. Cosmochim. Acta* **62**, 2863–2886 (1998).
5. M. Wiechert *et al.*, Oxygen isotopes and the Moon-forming giant impact. *Science* **294**, 345–348 (2001).
6. M. Touboul, T. Kleine, B. Bourdon, H. Palme, R. Wieler, Late formation and prolonged differentiation of the Moon inferred from W isotopes in lunar metals. *Nature* **450**, 1206–1209 (2007).
7. J. Zhang, N. Dauphas, A. M. Davis, I. Leya, A. Fedkin, The proto-Earth as a significant source of lunar material. *Nat. Geosci.* **5**, 251–255 (2012).
8. H. J. Melosh, An isotopic crisis for the giant impact origin of the Moon? *Meteorit. Planet. Sci. Suppl.* **72**, 5104 (2009).
9. J. Touma, J. Wisdom, Resonances in the early evolution of the Earth-Moon system. *Astron. J.* **115**, 1653–1663 (1998).
10. J. Wisdom, Z. Tian, Early evolution of the Earth-Moon system with a fast-spinning Earth. *Icarus* **256**, 138–146 (2015).
11. R. Rufu, R. M. Canup, "Evection resonance in the Earth-Moon system" in *44th Lunar and Planetary Science Conference*, S. J. Mackwell, E. K. Stansbery, D. S. Draper, Eds. (Universities Space Research Association Houston, Houston, TX, 2019), p. 3029.
12. Z. Tian, J. Wisdom, L. Elkins-Tanton, Coupled orbital-thermal evolution of the early Earth-Moon system with a fast-spinning Earth. *Icarus* **281**, 90–102 (2017).
13. M. Ćuk, D. P. Hamilton, S. J. Lock, S. T. Stewart, Tidal evolution of the Moon from a high-obliquity, high-angular-momentum Earth. *Nature* **539**, 402–406 (2016).
14. W. R. Ward, R. M. Canup, Origin of the Moon's orbital inclination from resonant disk interactions. *Nature* **403**, 741–743 (2000).
15. K. Pahlevan, A. Morbidelli, Collisionless encounters and the origin of the lunar inclination. *Nature* **527**, 492–494 (2015).
16. K. Atobe, S. Ida, Obliquity evolution of extrasolar terrestrial planets. *Icarus* **188**, 1–17 (2007).
17. S. Tremaine, J. Touma, F. Namouni, Satellite dynamics on the Laplace surface. *Astron. J.* **137**, 3706–3717 (2009).
18. M. L. Lidov, The evolution of orbits of artificial satellites of planets under the action of gravitational perturbations of external bodies. *Planet. Space Sci.* **9**, 719–759 (1962).
19. Y. Kozai, Secular perturbations of asteroids with high inclination and eccentricity. *Astron. J.* **67**, 591–598 (1962).
20. J. Touma, J. Wisdom, Evolution of the Earth-Moon system. *Astron. J.* **108**, 1943–1961 (1994).
21. P. Goldreich, History of the lunar orbit. *Rev. Geophys.* **4**, 411–439 (1966).
22. W. F. Bottke, R. J. Walker, J. M. D. Day, D. Nesvorny, L. Elkins-Tanton, Stochastic late accretion to Earth, the Moon, and Mars. *Science* **330**, 1527–1530 (2010).
23. S. Marchi *et al.*, Widespread mixing and burial of Earth's Hadean crust by asteroid impacts. *Nature* **511**, 578–582 (2014).
24. R. Brasser, S. J. Mojzsis, S. C. Werner, S. Matsumura, S. Ida, Late veneer and late accretion to the terrestrial planets. *Earth Planet Sci. Lett.* **455**, 85–93 (2016).
25. H. Genda, R. Brasser, S. J. Mojzsis, The terrestrial late veneer from core disruption of a lunar-sized impactor. *Earth Planet Sci. Lett.* **480**, 25–32 (2017).
26. R. Brasser, S. C. Werner, S. J. Mojzsis, Impact bombardment chronology of the terrestrial planets from 4.5 Ga to 3.5 Ga. *Icarus* **338**, 113514 (2020).
27. J. Wisdom, M. Holman, Symplectic maps for the N-body problem. *Astron. J.* **102**, 1528–1538 (1991).
28. W. M. Kaula, Tidal dissipation by solid friction and the resulting orbital evolution. *Rev. Geophys.* **2**, 661–685 (1964).
29. E. M. A. Chen, F. Nimmo, Tidal dissipation in the lunar magma ocean and its effect on the early evolution of the Earth-Moon system. *Icarus* **275**, 132–142 (2016).
30. G. J. Sussman, J. Wisdom, *Structure and Interpretation of Classical Mechanics* (MIT Press, Cambridge, MA, ed. 2, 2015).
31. K. J. Zahnle, R. Lupu, A. Dobrovolskis, N. H. Sleep, The tethered Moon. *Earth Planet Sci. Lett.* **427**, 74–82 (2015).